UCSF

UC San Francisco Electronic Theses and Dissertations

Title

Incorporating Metabolic and Physiologic Imaging into Radiation Therapy Treatment Planning of Patients with Glioblastoma

Permalink

https://escholarship.org/uc/item/2qm3q2x1

Author

Su, Guanzhong

Publication Date

2018

Peer reviewed|Thesis/dissertation

Incorporating Metabolic and Physiologic Imaging
into Radiation Therapy Treatment Planning
of Patients with Glioblastoma

by

Guanzhong Su

THESIS

Submitted in partial satisfaction of the requirements for the degree of

MASTER OF SCIENCE

in

Biomedical Imaging

in the

Acknowledgments

I am very grateful to my supervisor Dr. Janine Lupo whose expertise, guidance and support allowed me to work on such an interesting topic. Thanks for supervising and giving valuable feedback regarding the research, which laid a solid foundation for my future. I am largely indebted to Maryam Vareth for suggestions on compiling essential clinical data, who provided valuable help and insight in analyzing brain images by using MATLAB. I would like to thank Dr. Steve Braunstein, Dr. Javier Villanueva-Meyer, and Dr. Olga Tymofiyeva for taking time out of their hectic schedules to be a part of my thesis committee and provide feedback. Thanks to all members in Lupo lab for their suggestion and great help during the thesis. Additional thanks to the MSBI program administrators and faculty for providing me with this wonderful education. Finally, thank you to my classmates for making this program an enjoyable experience.

Dedication

I would like to dedicate this to my parents for providing moral and financial support.

Incorporating Metabolic and Physiologic Imaging into Radiation Therapy Treatment Planning of Patients with Glioblastoma

Guanzhong Su

Abstract

Glioblastoma (GBM) remains the most aggressive cancer of the brain. Typical survival in patients with GBM is around 12-18 months, due to local or distant recurrence that occurs even after treatment with radiation and chemotherapy. Although there have been improvements in modern imaging, the radiation planning protocols are still based purely on a 2 cm geometric expansion of conventional post-contrast T1-weighted and T2-weighted FLAIR anatomic sequences. As a result, about 60% of tissue within the high dose treatment field can be normal brain tissue, which can damage to healthy brain function, while microscopic disease farther from the primary tumor bed is untreated. The main goal of this project was to develop a pipeline for the integration of probability maps derived from metabolic and diffusion-weighted MRI into the clinical workflow for radiation treatment planning. 24 patients with newly-diagnosed glioblastoma, who had undergone RT and chemotherapy consisting of an anti-angiogenic agent, were scanned at baseline prior to therapy and had serial follow-up imaging every 2 months until progression. Four patients were excluded because of either a poor initial model fit that resulted in inaccurate probability maps or poor image quality at the time of progression, leaving a total of 20 patients for evaluating our automatic contouring algorithm. First, we determined the optimal threshold for each

patient's probability map based on ROC analysis of the overlap of probability map with the progressed lesion. This value was then projected back on the histogram to automatically calculate each patient's threshold based on the individual patient's histogram and a maximum distance cutoff of 5 cm based on standard clinical procedures of high dose delivery during RT planning. Our results show that we were able to develop an automated contouring routine for integration of metabolic and physiology imaging into clinical workflow for radiation treatment planning. Incorporating a maximum distance from the original lesion allowed the automatic selection of a threshold from a consistent position on the histogram of the probability maps that optimized the overlap with the progressed lesion.

Table of Contents

List of Tables

List of Figures

CHAPTER 1

INTRODUCTION

1.1 Radiation Therapy and the Treatment of Glioblastoma

Despite advances in radiation therapy that have improved survival in patients with malignant brain tumors, glioblastoma (GBM) remains the second most common brain tumor, after meningioma, and the most aggressive cancer that originates within the brain [1] [2]. Typical survival in patients with GBM is around 12-18 months [3], due to local or distant recurrence that occurs despite surgical resection followed by treatment with radiation and chemotherapy with temozolomide (TMZ) which has become the standard of care.

Although there have been improvements in modern imaging, and RT delivery systems that can now precisely deliver high dose radiation to a highly complex-shaped tumor region, radiation planning protocols (Figure 1.) are still based purely on a 2 cm uniform geometric expansion of lesions defined on conventional anatomical images, which includes post-contrast T1-weighted and T2-weighted FLAIR anatomic sequences. This is because approximately 90% of GBMs treated with standard-of-care therapy have been found to progress within 2cm away from the original tumor bed [11].

As a result, about 60% of tissue within the high dose treatment field can be normal brain tissue [8], which can damage healthy brain function, while microscopic infiltrating disease farther from the original tumor bed can go untreated in treatment planning. In other words, the current standard RT planning approach can both miss treating with the maximum dose of radiation areas

that are more likely to recur, as well as over-treated uninvolved normal tissue.
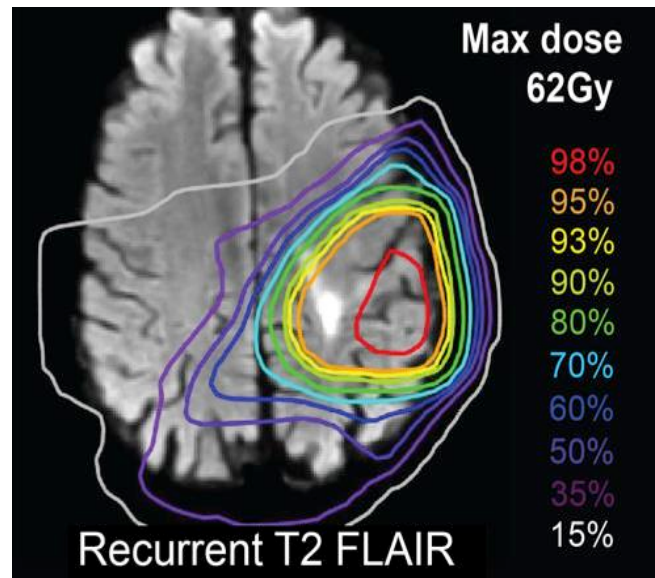
Figure 1. Original dosimetry radiation planning protocol for GBM patients.

1.2 The Role of Advanced Physiologic and Metabolic MR Imaging

MRI is an effective tool for visualization, diagnosis, and making treatment planning for GBM patients. Advanced physiologic and metabolic MRI are able to visualize cellular-level tumor involvement [5] [6]. Increased Apparent Diffusion Coefficient (ADC) represents more edema while decreases reflect areas that are more cellular. Decreased Fractional Anisotropy (FA) reflects subclinical invasion that results and decreased directionality along white matter. Dynamic Susceptibility-Contrast (DSC) perfusion-weighted imaging (PWI) is a good method for probing the brain's vascularity, through measurements of relative cerebral blood volume (rCBV) and vessel leakiness. ^{1}H MR spectroscopic imaging (MRSI) provides metabolic information through the Choline to NAA index (CNI) and levels of lactate and lipid, which can identify differences of cellular

metabolism, hypoxia, and necrosis between normal and tumor cells [4]. Incorporating these

advanced MR techniques may provide more information on the spatial characterization of high-

grade gliomas and aid in the planning of subsequent treatments [7] [8], with the goal of ultimately

improving overall survival [9].

1.3 Prior results for Incorporating Advanced Imaging into Dosimetry Planning

Several studies have explored how to incorporate advanced imaging modalities into RT

planning for patients with GBM. In a previous study, our group has shown that incorporating

parameters derived from metabolic and diffusion MRI at the time of radiation therapy can be used

to predict regions of subsequent recurrence [4]. Figure 2 shows the equation of the model that

provided a likelihood of recurrence probability score per voxel based on the diffusion (ADC, FA),

spectroscopy (CNI), distance from the edge of the baseline tumor volume and radiation dose.

Figure 3 shows an example of a likelihood of recurrence or probability map.

$$
\begin{aligned}
group \sim\ & 1\,|\ FA + ADC + CNI + I\!\left(\frac{1}{dose\ \times\ min\_dist}\right) \\
& + I\!\left(\frac{CNI}{dose\ \times\ min\_dist}\right) + I\!\left(\frac{ADC}{dose\ \times\ min\_dist}\right) \\
& + I\!\left(\frac{FA}{dose\ \times\ min\_dist}\right).
\end{aligned}
$$

Figure 2. Continuous model for calculating the probability of recurrence
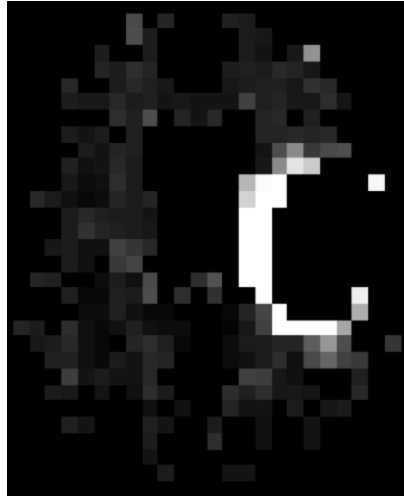
Figure 3. Example slice of a probability map for an example patient

1.4 Receiver Operating Characteristic (ROC) curves

The Receiver Operating Characteristic (ROC) curve is a plot of sensitivity vs. false positive rate (1-specificity), for a range of diagnostic test results [10] (Figure 4). It graphically represents the compromise between sensitivity and specificity in tests which produce results on a numerical scale. It therefore allows a graphical representation of a test's accuracy and may be used to generate decision thresholds or "cut off" values. This means we can use this approach to determine optimal thresholds that can be applied to future cohorts. Here, we define terms consisting of four outcomes, which come from true progression and probability prediction. The four outcomes are described by a 2×2 contingency table (Table 1.) and the figure shown below:

Table 1. Definition of four outcomes

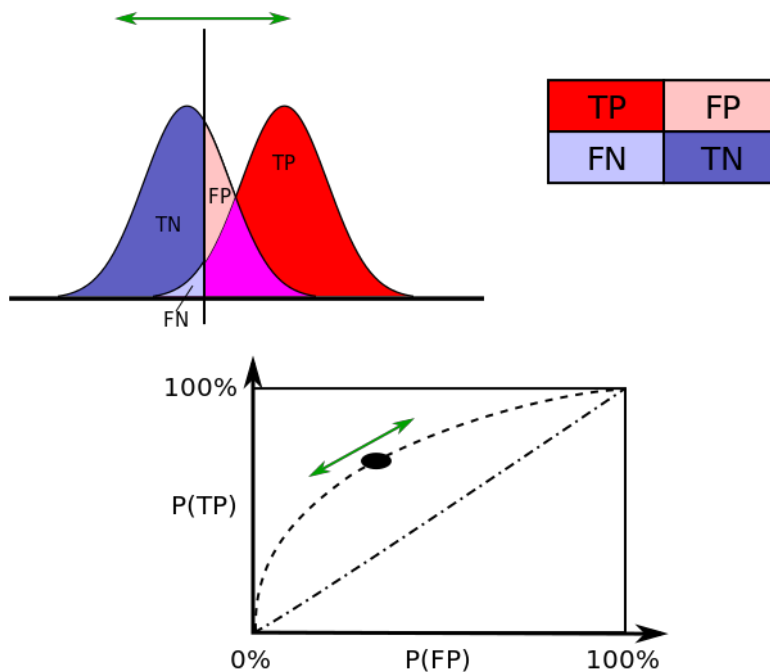|	*True*	Progression Mask (TRUTH)	
Predict		√	×
Probability Mask (TEST) — √	√	√ Progression √ Probability Volume 1 *True Positive (TP)*	× Progression √ Probability Volume 2 *False Positive (FP)*
Probability Mask (TEST) — ×	×	√ Progression × Probability Volume 3 *False Negative (FN)*	× Progression × Probability Volume 4 *True Negative (TN)*

Figure 4. Simple example of ROC curve with moving cutoff point

1.5 Motivation

Although there are several studies that explore the feasibility and utility of incorporation

of advanced imaging modalities into RT planning for patients with GBM, clinical radiation planning

target volumes are still defined by a 2 cm geometric expansion of the T2-hyperintensity lesion

from a T2-weighted FLAIR anatomic imaging sequence that is not specific to tumor. Our group

and others have shown that metabolic and/or diffusion MRI techniques before radiation therapy

can be used to predict regions of subsequent recurrence and should thus be integrated with

current RT planning strategies.

1.6 Objective

The main goal of this project was to develop a pipeline for integration of   probability

maps derived from metabolic and diffusion-weighted MRI into the clinical workflow for radiation

treatment planning by: 1) automatically calculating appropriate thresholds of likelihood of

recurrence (probability) maps for contouring in treatment planning system; 2) removing low risk

regions, which should be spared, while keeping all areas at high risk which need to be treated; 3)

maintaining the accuracy of the processed probability map to predict regions of tumor progression.

CHAPTER 2

MATERIALS AND METHODS

2.1 Patient population

24 patients with newly-diagnosed glioblastoma, who had undergone RT and chemotherapy consisting of temozolomide and an anti-angiogenic agent (enzaustaurin or avastin) were included in this IRB approved study. The median age of the patients was 52 years old, range = 25 to 70 years old. Only patients with a Karnofsky performance score equal or greater than 60 could be enrolled in this study, and patients who discontinued therapy were excluded [4]. All patients had serial follow-up imaging every 2 months until progression. Figure 5 shows anatomical images and corresponding contrast enhancing lesion (CEL) and T2-hyperintensity lesion (T2L) ROIs for a representative patient before RT and at the time of progression, as well as the likelihood of recurrence or "probability" map. Four patients were excluded due to either poor model accuracy when generating the probability maps or extremely poor image quality at the time of progression, leaving a total of 20 patients for developing a method for automatic contouring of probability maps.

2.2 Images utilized

T1-weighted spoiled gradient echo (SPGR) images post-injection of a gadolinium (Gd) based contrast agent and T2-weighted fluid attenuated inversion recovery (FLAIR) images that were acquired pre-RT and at the time of progression, were used in conjunction with probability maps that were created using diffusion and metabolic imaging parameters. Two types of lesions

were drawn on these images [4]. The first region of interest (ROI) was the contrast enhancing lesion (CEL), which was manually defined on the co-registered post-Gd T1 SPGR images, excluding enhancement that was also present on the pre-Gd T1 images. The second was the T2-hyperintense lesion (T2L), which was segmented based on the hyperintense signal on FLAIR images using a semiautomatic method [12] developed in our laboratory.

a) Original Tumor Maps

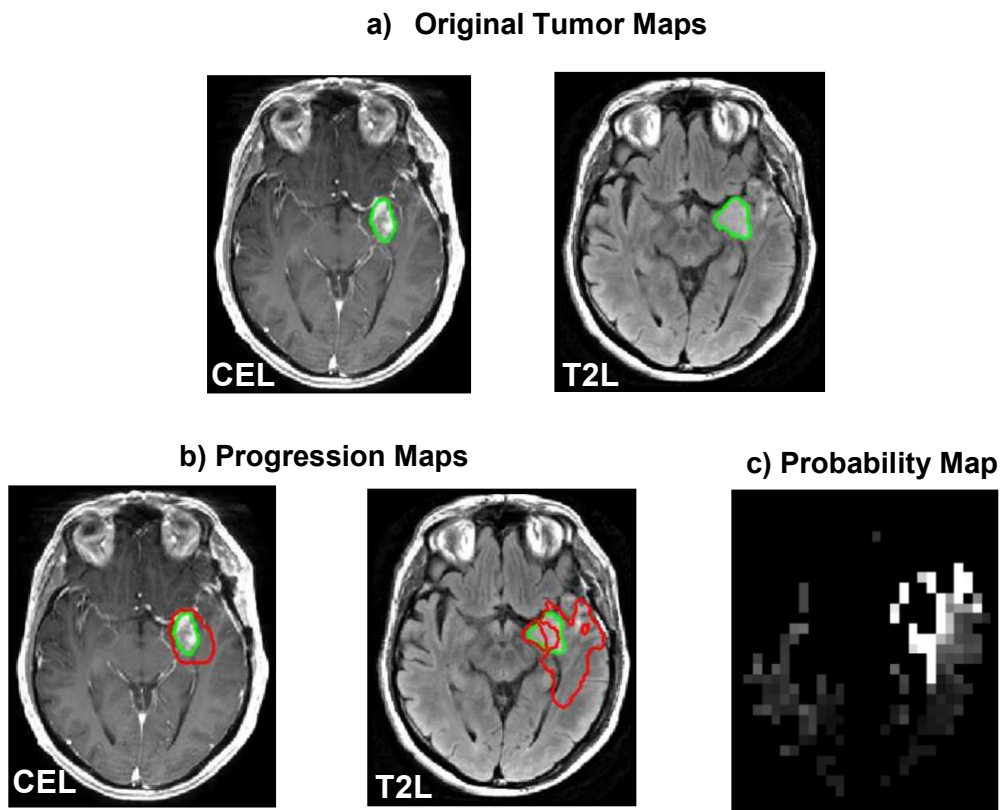**b) Progression Maps**   **c) Probability Map**

Figure 5. An example of a) anatomical images of the original tumor, b) at the time of progression and c) probability of progression map.
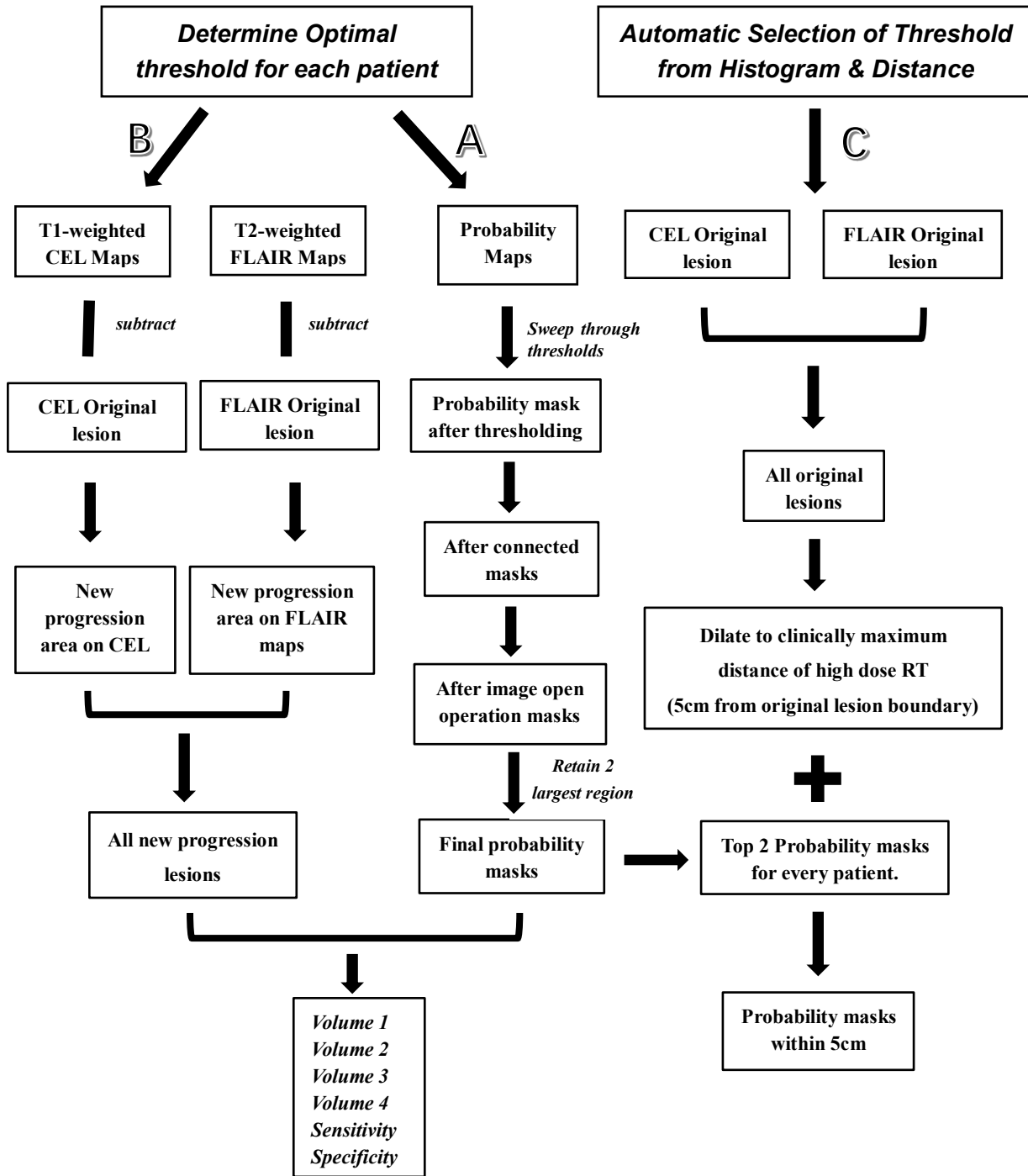
Figure 6. Data processing pipeline

2.3 Determining the Optimal Threshold for Each Patient

As illustrated in Figure 6, preliminary postprocessing of probability maps can be separated to two steps. The first step was implemented to determine each patient's optimal threshold based on ROC analysis of the overlap of the thresholded probability map using a range of thresholds, with the progressed lesion. The reason to threshold the probability maps is that there is a mass of zero points and a lot of low risk regions, which should be spared, while keeping all areas of high risk which should be treated. In branch A, we use MATLAB (version of 2017a) to find multiple potential thresholds for the probability map of each patient by creating a histogram of intensity values of each patient's probability map. This histogram is divided into 100 blocks and the most significant changes between mean values of adjacent blocks were quantified (Figure 7a.). The 14 most significant of the 100 change points, which correspond to the 100th, 99th, 98th, 97th, 96th, 90th, 80th, 70th, 60th, 50th, 40th, 30th, 20th, 10th percentiles as our threshold value and make binary masks for probability maps (Figure 7b.).

After the initial threshold process, a total of 14 masks were obtained for every patient (Figure 8a.). The second step was then to search for 3D regions in the thresholded probability maps obtained from the previous step and remove all unconnected regions that had fewer than __ voxels. Connectedness was defined as sharing a face, edge, or corner, with a neighboring voxel. where all single voxels would be removed from masks. Finally, only the 2 largest regions in each probability map were retained as shown in Figure 8b.
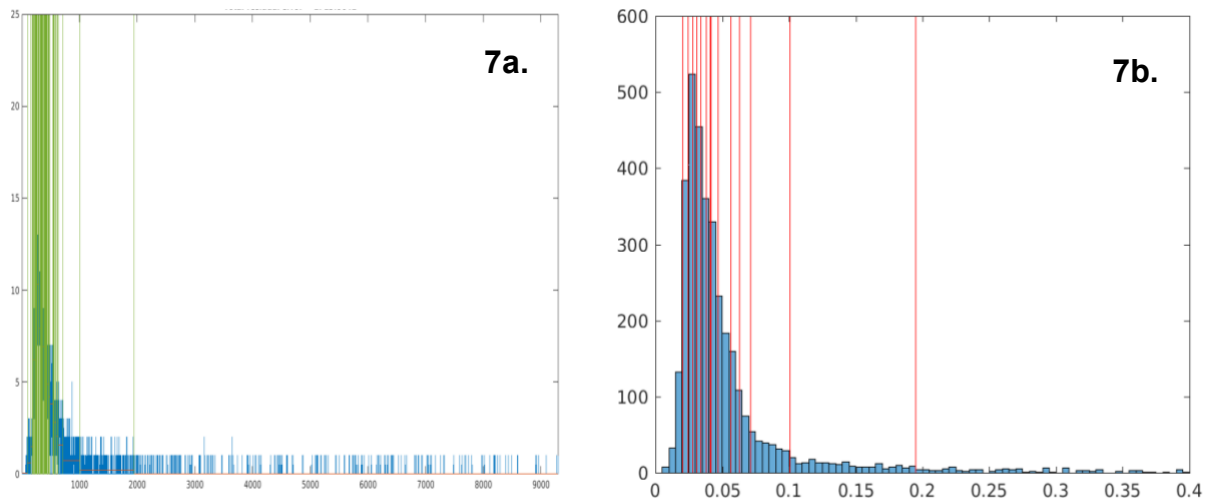
Figure 7. Histogram and thresholds. An example of one patient's (patient # b2167) probability map histogram with 100 significant change points showed in green line (7a), and 14 thresholds show in red line on histogram (7b).
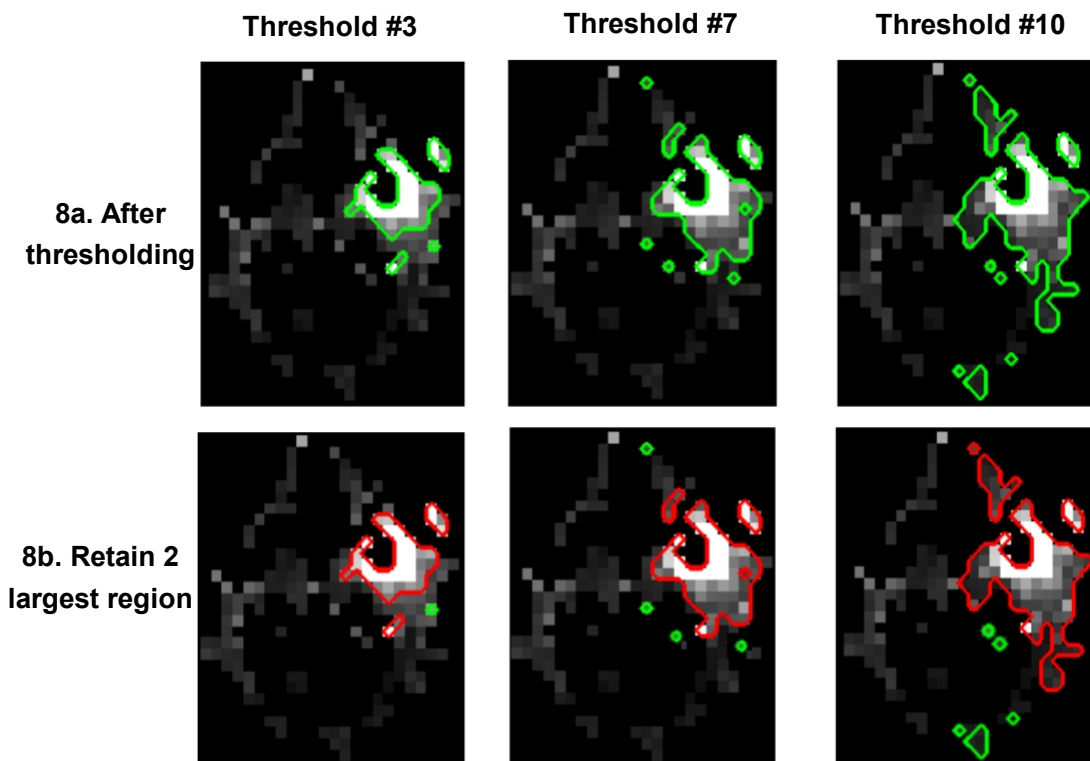
Figure 8. Pipeline for thresholding. A representative slice of a probability map after thresholding by 3 thresholds (#3, #7, #10) and displaying the contours on the original probability map, shown in green (8a); The same slice of final probability map with 2 largest regions shown in red (8b).

As shown in branch B of Figure 6, a new progression region is first obtained by subtracting the original lesion region from the new lesion on each of the T2L and CEL masks (Fig. 9). The new progression region on the T2L and CEL masks are then combined (Fig. 9c). These steps make sure that we only include any new regions of tumor in our analyses.
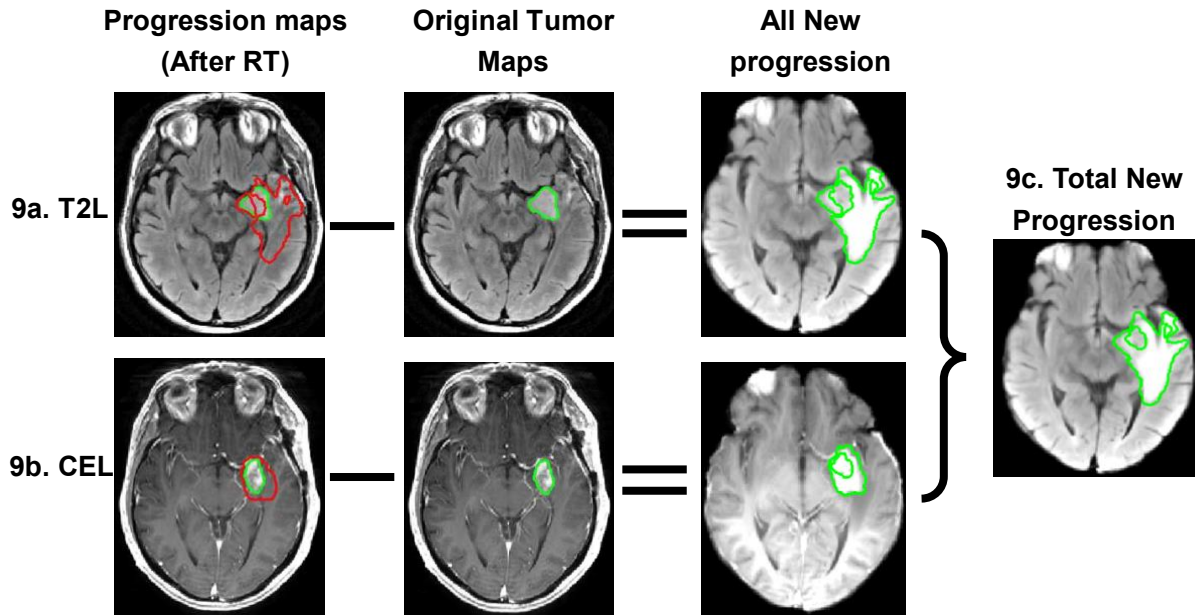
**Figure 9.** Pipeline for generation of new progression region. Slice 37 of patient b2167 of all new progression lesion on T2L mask showing in green contour line (9a); The same slice of new progression lesion on CEL mask display in green line (9b); And the total new progression region with green boundary (9c) by combining 9a and 9b.

2.4 ROC analysis of the overlap of probability maps with progressed lesions

In order to qualitatively and quantitatively evaluate the accuracy of our 14 thresholded probability masks in predicting the region of progression, we needed to calculate the volume of true progression that is correctly covered (or predicted) by the thresholded probability map (Volume 1, Fig 10), and the volume of true progression that does not overlap with the thresholded

probability map (Volume 3, Fig 10). Because new progression masks (FOV = 180mm * 240mm * 150mm, Matrix Size = 192 * 256 * 50) and probability maps (FOV = 180mm * 240mm * 150mm; Matrix Size = 36 * 48 * 50) were created at different resolutions, we up-sampled the thresholded probability masks to the size of the progression masks using nearest neighbor interpolation to retain the binary information. Otsu's method was then used to choose the threshold value that minimized the intraclass variance of the thresholded black and white pixels [13]. The up sampled probability masks were then used to calculate different volumes, sensitivity and specificity values for 14 unique thresholds for each patient as described in Figure 10.

Volume 1 = New progression mask ∩ thresholded probability map

(Mean volume both of progression mask and thresholded probability map)

Volume 2 = Probability mask – Volume 1

(Mean volume of the thresholded probability map that is not within the progression mask.)

Volume 3 = New progression mask – Volume 1

(Mean volume of the progression mask that is not within the thresholded probability map)

Volume 4 = Brain volume – [New progression mask ∪ Probability mask]

(Mean volume that is neither in the progression mask nor the thresholded probability map)

The sensitivity and specificity are given by the following equation:

$$\text{Sensitivity} = \frac{Volume\ 1}{Volume\ 1 + Volume\ 3};$$

$$\text{Specificity} = \frac{Volume\ 4}{Volume\ 4 + Volume\ 2};$$
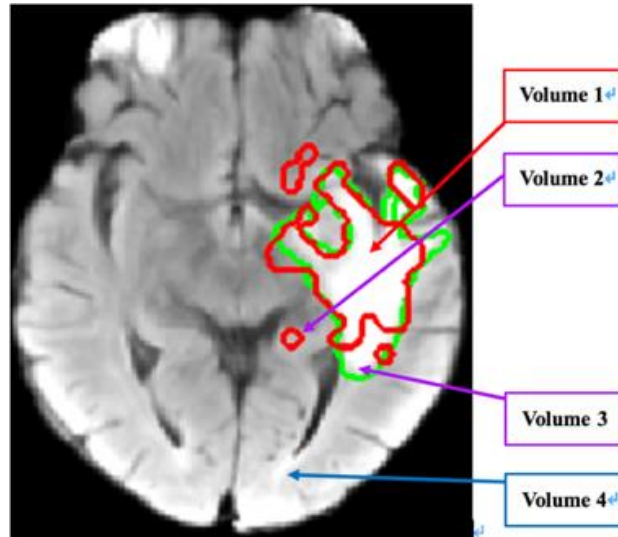
Figure 10. Brief illustration of different volumes. (Image from patient b2167, slice 35)

Figure 11 shows ROC curves for 20 patients generated by 14 different thresholds for each patient. Each color represents one patient, and the last point of each curve represents the entire non-thresholded probability map.
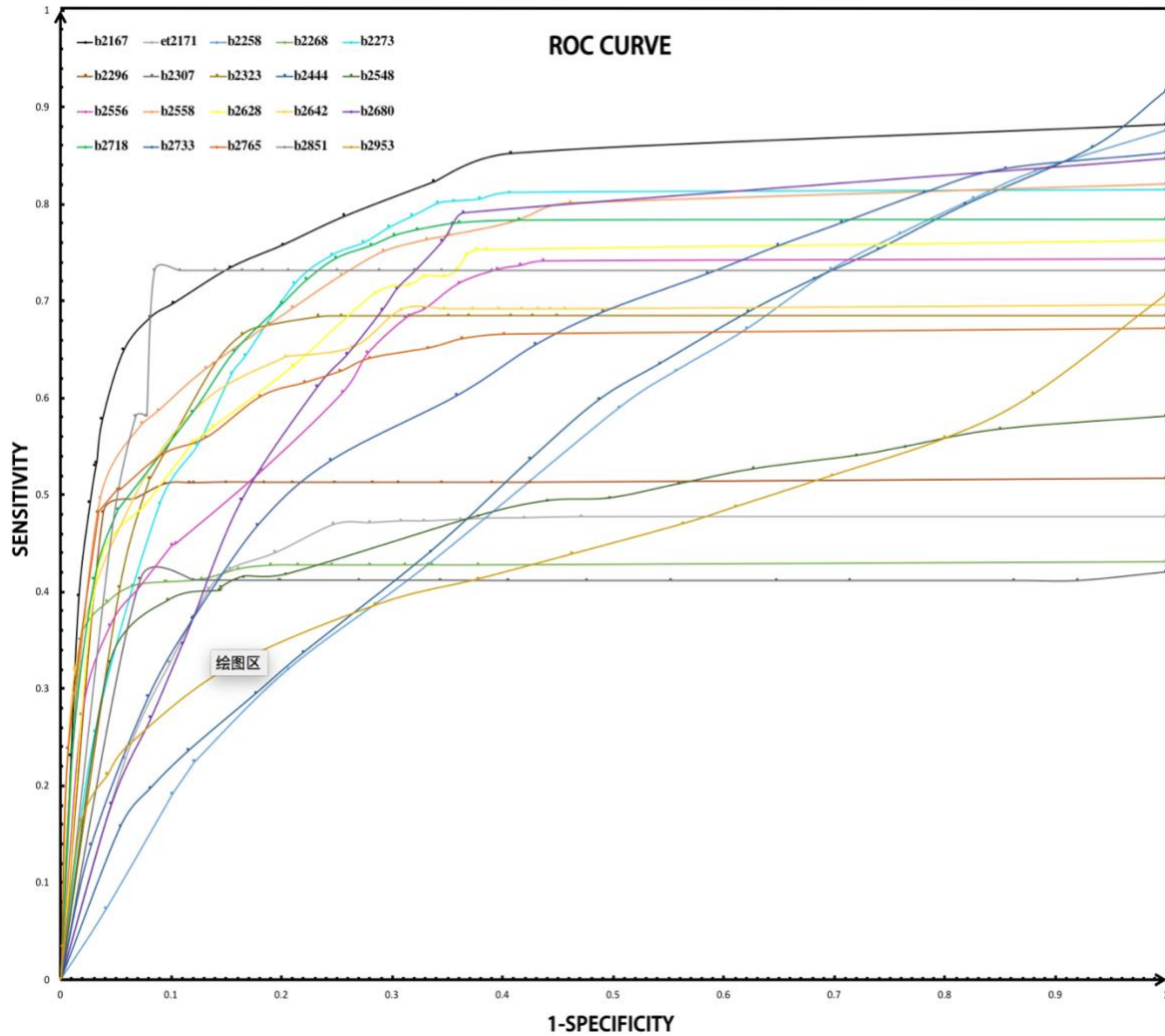
Figure 11. The ROC curve for 20 patients, where x-axis is false positive rate (1-specificity), and y-axis is sensitivity value.

Since the goal was to use the ROC curves shown in Figure 11 to find the optimal threshold for each patient, we used a method that gives equal weight to sensitivity and specificity as showing in Figure 12, where S_n and S_p represent sensitivity and specificity, respectively, and the distance (d) between the point (0, 1) and any point on the ROC curve is:

$$d = \sqrt{[(1 - S_n)^2 + (1 - S_p)^2]}$$

To get the optimal cutoff point on ROC curves that can best discriminate the high-risk recurrence voxels with low-risk recurrence or no risk recurrence voxels, d was calculated for 15 observed cut-off points in order to locate the point where the distance to the top left corner (0,1) in ROC space is minimized.

Figure 12. Finding the optimal threshold from an ROC curve [20].

Table 2 and Table 3 summarize the optimal threshold # and threshold value for each patient, and Figure 13a shows where we initially expected the optimal threshold to be on the histogram, while Figure 13b and 13c show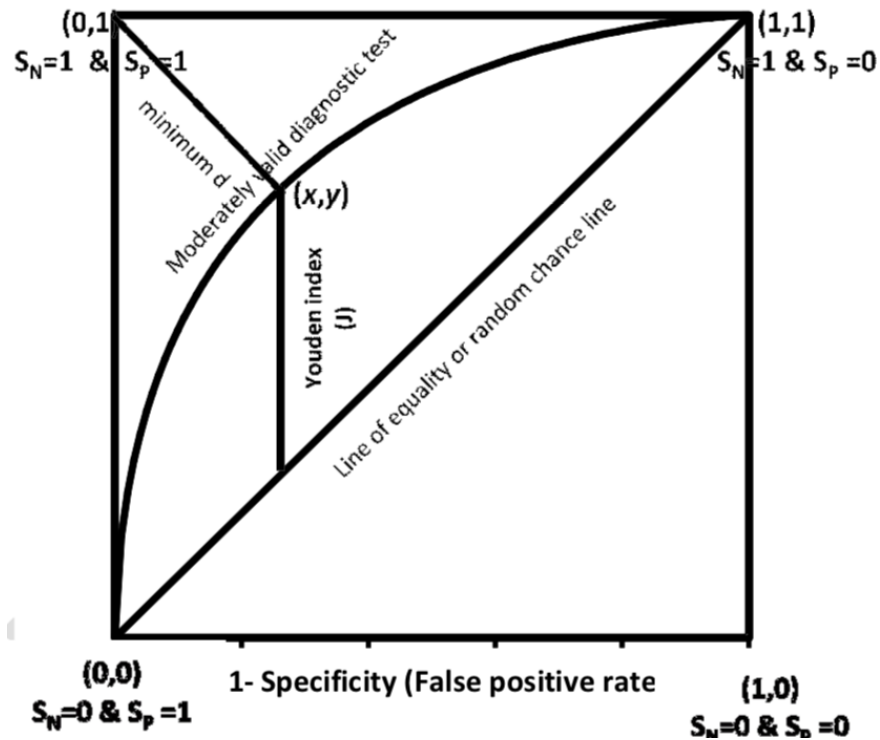 two other common optimal threshold positions: Right FWHM (Full Weight at Half Maximum) (Figure 13b), and Peak (Figure 13c).

Table 2. Optimal threshold summary

Patients_b number	Optimized Thresh number from ROC	Thresh_value	Position_optimized thresh
b2167	10	0.034	Peak
et2171	7	0.1125	Right FWHM
b2258	8	0.0493	Peak
b2268	3	0.1005	Expected
b2273	7	0.0525	Right FWHM
b2296	3	0.0671	Expected
b2307	1	0.1273	Expected
b2323	5	0.1231	Expected
b2444	7	0.0475	Right FWHM
b2548	5	0.0971	Expected
b2556	9	0.0614	Peak
b2558	7	0.055	Right FWHM
b2628	7	0.0604	Right FWHM
b2642	4 or 5	0.1039	Expected
b2680	13	0.0295	Peak
b2718	8	0.068	Peak
b2733	6	0.0826	Right FWHM
b2765	8	0.0587	Peak
b2851	5	0.0633	Expected
b2953	7	0.0511	Right FWHM

Table 3. Number of optimal threshold positions

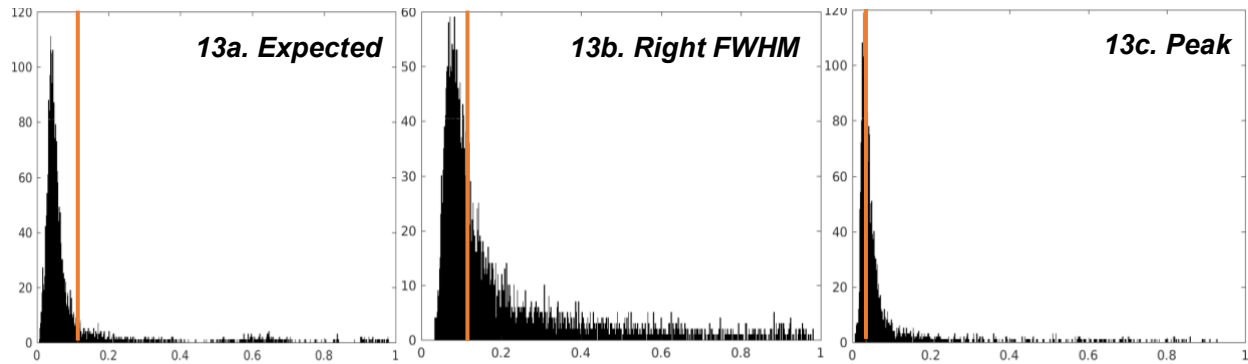| Threshold Position	Amount
Right FWHM	7
Peak	6
Expected	7
Total	20

Figure 13. Summary of optimal thresholds (yellow line) showing on histogram, a. expected position; b, Right FWHM position; c, Peak position.

Figure 14 shows one slice of three different patients T2 FLAIR images overlaid with true progression region (red contour line) and probability map (green contour line) from 3 different values obtained from histogram analysis: expected, Right FWHM and Peak position thresholds. For the first patient (b2167), if we used the expected and Right FWHM thresholds, we would have underestimated the region of progression (green contour). However, if we used the Peak threshold the region of progression will be overestimated. Similarly, for the other patients, the expected threshold will underestimate the recurrence region, while the Right FWHM and Peak thresholds will greatly overestimate the region of progression. From these examples, we realized that some measure of distance from the lesion must be incorporated to be able to automatically select an appropriate threshold value based on a patient's histogram.
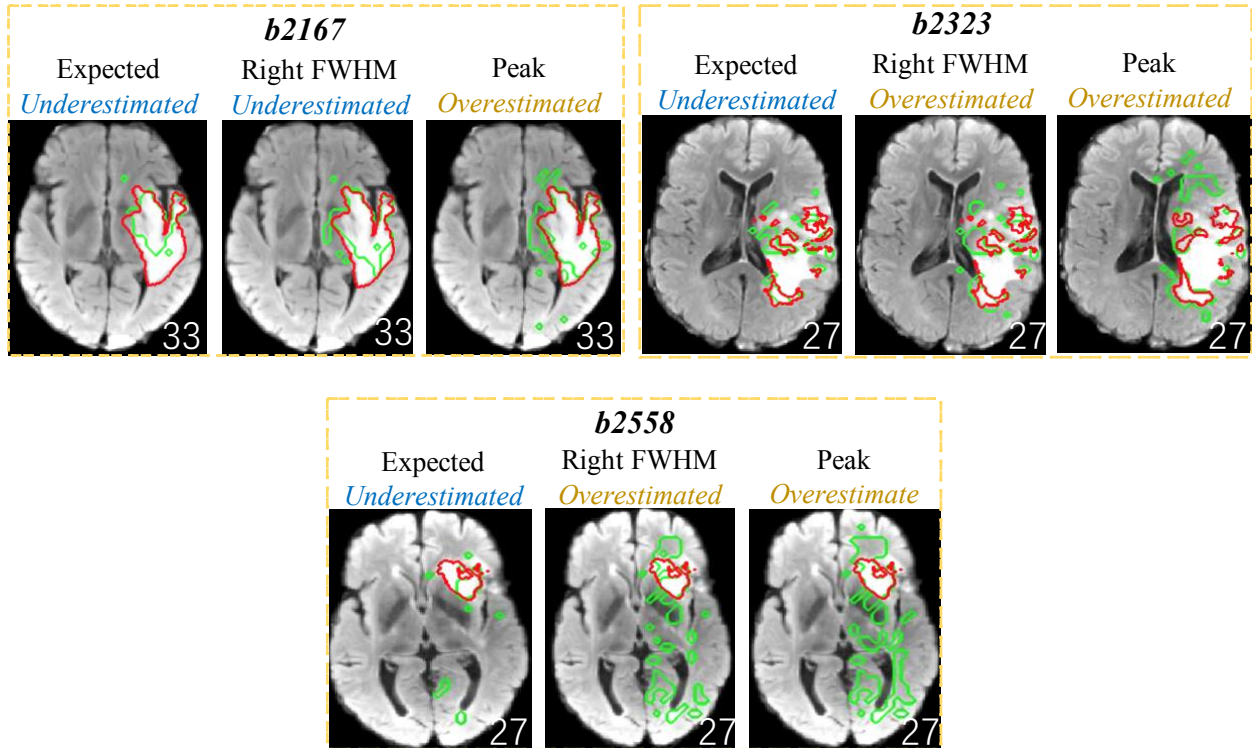
Figure 14. Three examples of the overlap of the thresholded probability map with the progressed lesion. Background is T2 FLAIR image after RT, green contour line is probability mask, and red contour line is the region of true progression map.

2.5 Automatic Selection of Threshold from Histogram & Distance

The second goal of this project was to automatically calculate thresholds based on an individual patient's histogram and the maximum clinically allowable distance of high dose RT. As shown in Figure 5 branch C, we first combine the original T2L and CEL lesions, followed by another operation that dilates the binary lesion masks by 50 voxels in every direction out to 5cm. The final thresholded probability map is obtained by masking the processed probability map with the dilated T2L mask an overlaid as a contour (Figure 15).

FLAIR Original lesion

CEL Original lesion

Combined Original Lesion

After dilating

Final Probability Masks within 5cm
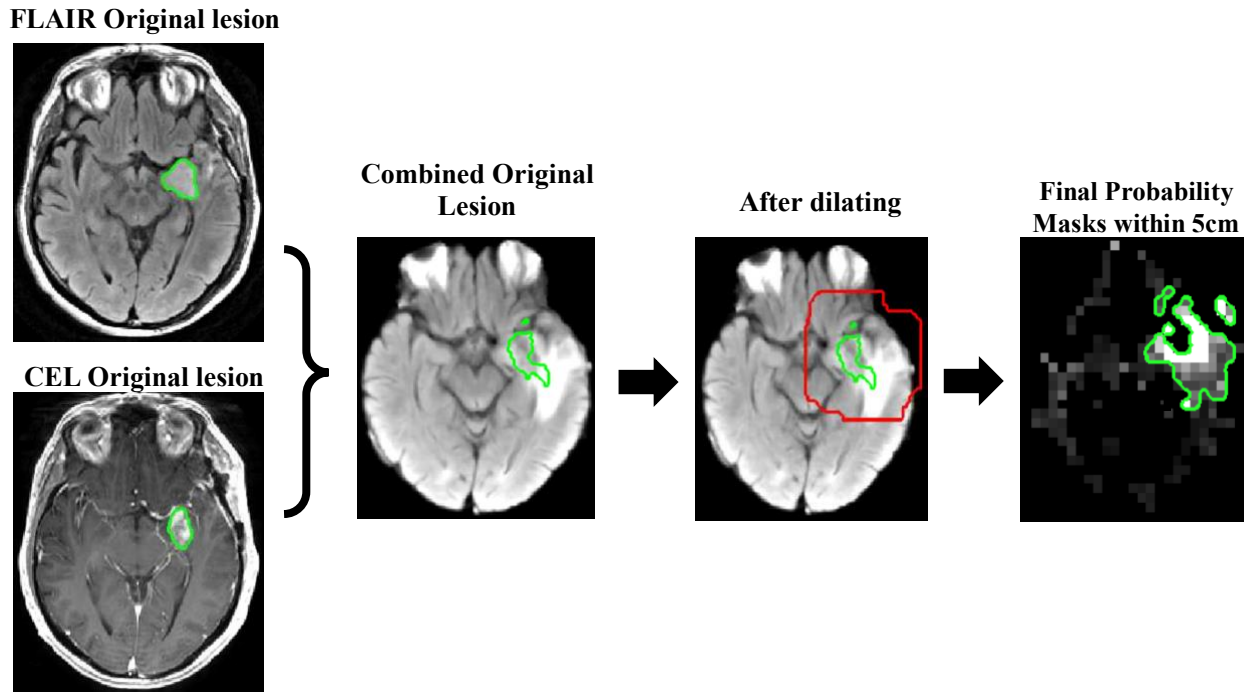
Figure 15. Combination of CEL and T2L original lesions to obtain original lesion (green contour line) that is overlaid on the T2 FLAIR image at the time of progression. The original lesion is then dilated out to 5cm (red contour), which is used to constrain the final contoured probability maps (on right).

CHAPTER 3

RESULTS

3.1 New ROC curves

After obtaining our final thresholded new probability maps for each patient, we constructed new ROC curves as shown in Figure 16. The total area under the ROC curve (AUC) is a single index for measuring the performance of a test. The larger the AUC, the better the overall performance of the thresholded probability map to correctly predict future recurrent tumor and unaffected voxels. Figure 17 shows an original ROC curve compared to one obtained from the new optimized thresholding method for a representative patient (b2167). The new ROC curve (yellow line) has a larger AUC than the original one in blue. Incorporating a clinically defined maximum distance for the threshold contour improved the AUC for all patients.

3.2 New optimal thresholds for each patient

The results of the recalculated optimal threshold for each patient, and optimal threshold value and location on histogram are listed in Table 4. Table 5 shows the total number of patients exhibiting each threshold type. This time, there are 12 patients that have the Right FWHM location on the histogram as their optimal threshold, while 6 patients have the expected position, and only 2 patients have their optimum threshold located at the peak. As a result, Right FWHM was selected as the uniform threshold location for all the patients in this study, from which to threshold each patient's probability map.
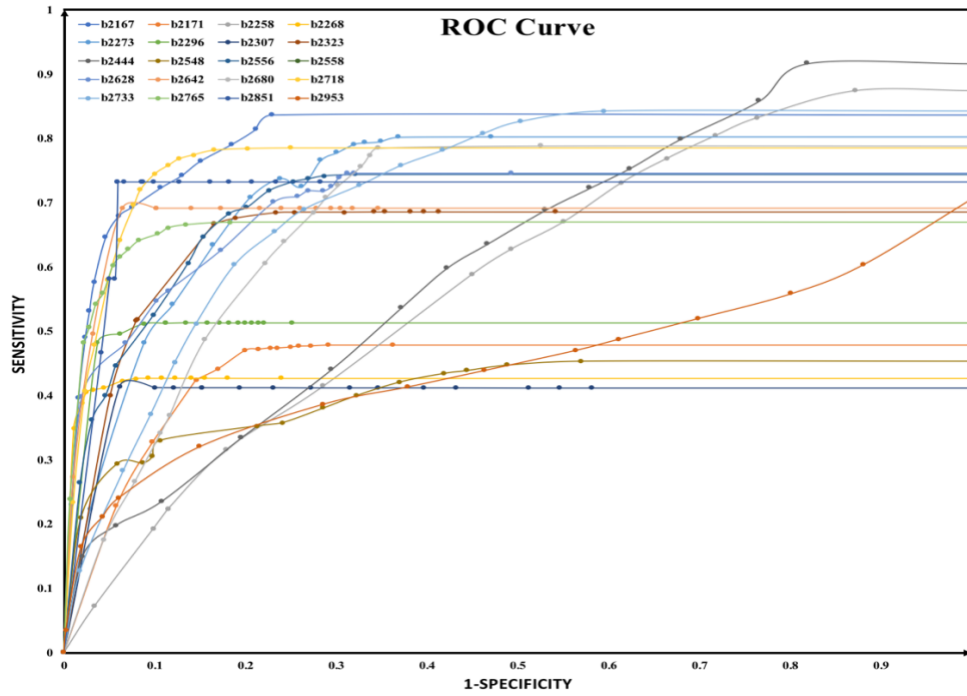
Figure 16. New ROC curves for 20 patients, where the x-axis is the false positive rate (1-specificity), and y-axis is sensitivity
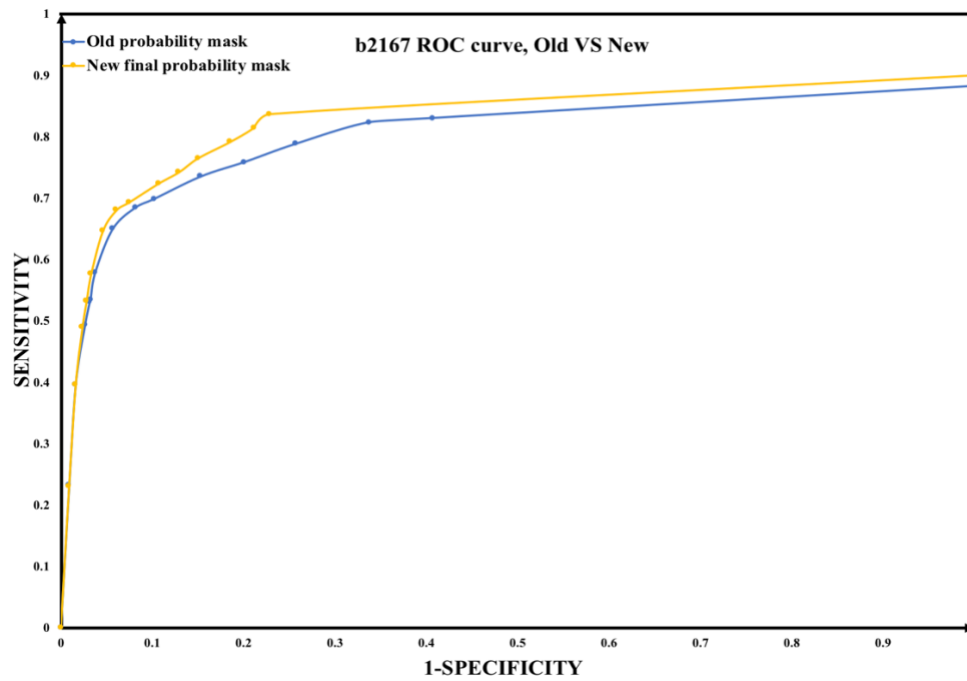

Figure 17. Comparison of old and new ROC curves for one patient

Table 4. New optimal threshold summary

Patients_b number	Optimized Thresh number from ROC	Thresh_value	Position_optimized thresh
b2167	13	0.0246	Peak
et2171	7	0.1125	Right FWHM
b2258	8	0.0493	Peak
b2268	8	0.0655	Right FWHM
b2273	7	0.0525	Right FWHM
b2296	6	0.0526	Right FWHM
b2307	1	0.1273	Expected
b2323	7	0.0826	Right FWHM
b2444	8	0.0435	Right FWHM
b2548	7	0.0597	Right FWHM
b2556	11	0.0519	Peak
b2558	9	0.0459	Right FWHM
b2628	7	0.0604	Right FWHM
b2642	3	0.1363	Expected
b2680	13	0.0295	Peak
b2718	11	0.0525	Peak
b2733	9	0.0541	Right FWHM
b2765	13	0.0403	Peak
b2851	6	0.0555	Right FWHM
b2953	7	0.0511	Right FWHM

Table 5. New number of each optimal threshold position

Threshold Position	Amount
Right FWHM	12
Peak	6
Expected	2
Total	20

3.3 Examples of new probability masks and improvements of sensitivity & specificity

Figure 18 shows two different patients with true progression region (red contour line) overlaid with the probability map generated by the original method (green contour line) compared to the new probability map (blue contour line). The new contours more accurately cover the entire region of tumor progression while simultaneously removing the isolated green regions of presumed normal brain tissue that are far away from the original tumor bed (considered a false positive).
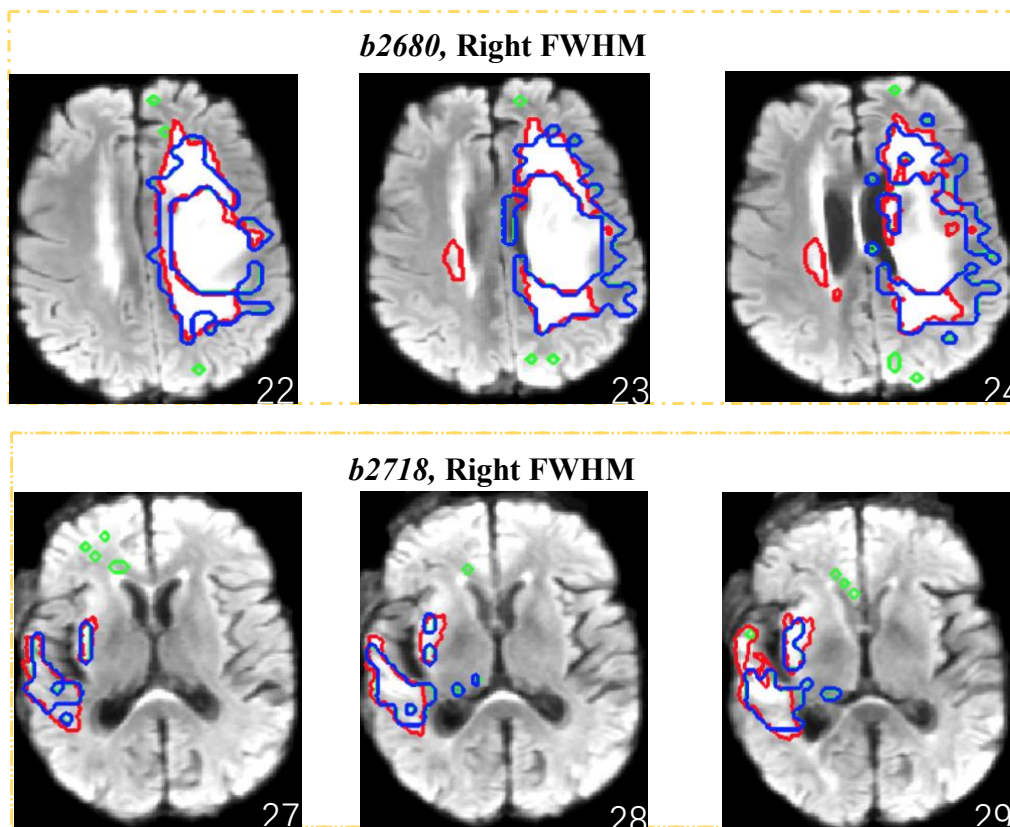

Figure 18. Two examples of the overlap of new probability contours with the progressed lesion. Background is the T2 FLAIR image at the time of progression while the green contour line used the original method, blue contour line is the result of the new method, and the red contour line is region of true progression.

Figure 19 shows the original thresholded sensitivity and specificity (blue columns) compared to the new optimal threshold sensitivity and specificity (orange columns) using the new probability maps masked to within 5cm of the original tumor boundary. The new method had significantly higher sensitivity (p=0.00465, Wilcoxon signed rank test) and specificity values (p=0.0139, Wilcoxon signed rank test) compared to the original method. However, the range of sensitivities and specificities varied substantially among patients (i.e. from 0.79 (b2167) to 0.41 (b2307) and 0.94 (b2851) to 0.55 (b2258), respectively), suggesting that the original prediction model could be improved.
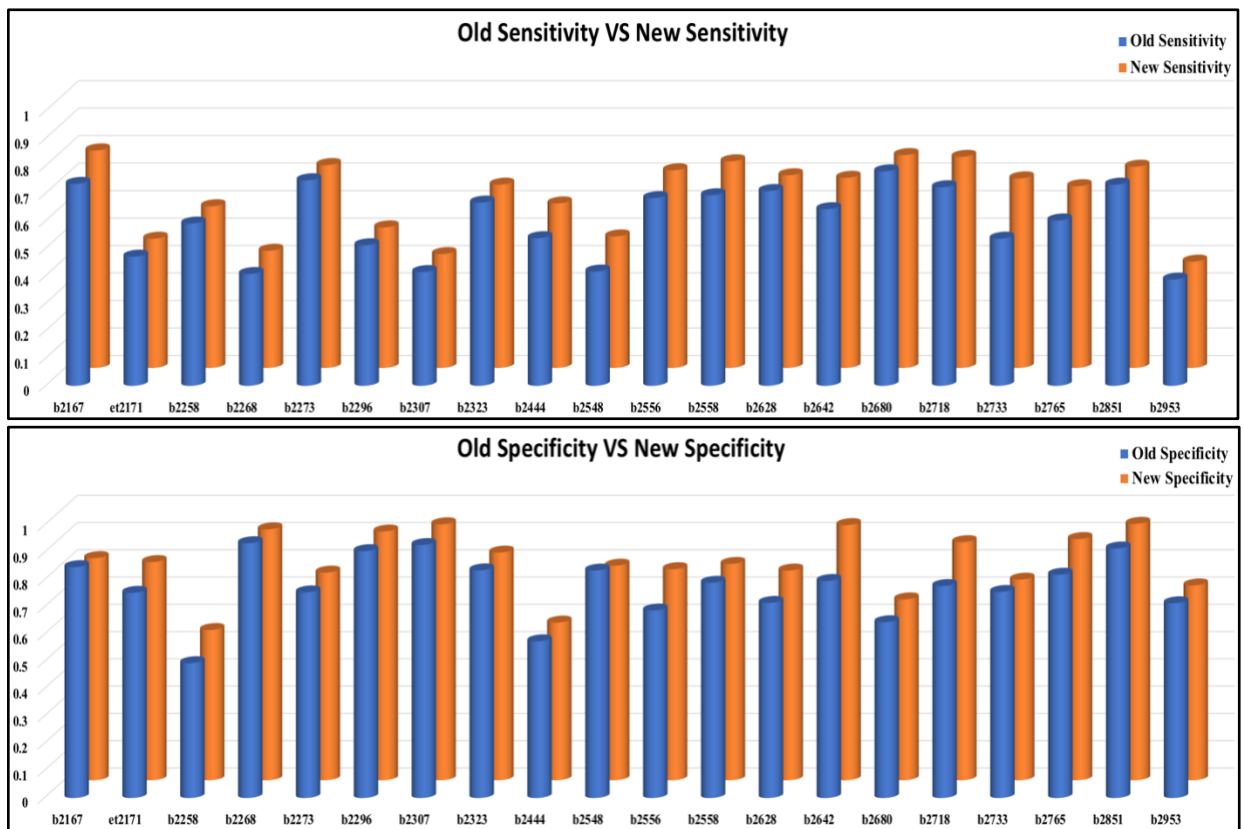

Figure 19. Comparison of original sensitivity and specificity (blue columns) with new sensitivity and specificity (orange columns).

CHAPTER 4

DISCUSSION

EBRT in conjunction with TMZ is a standard therapeutic regimen for extending survival of highly infiltrative, high-grade gliomas. Despite advances in modern imaging and accuracy of RT delivery systems, RT planning protocols are still based on a purely 2 cm uniform geometric expansion conventional anatomical images including post-contrast T1-weighted and T2-weighted FLAIR anatomic sequences. This kind of treatment planning can cause damage to healthy brain tissue and decrease quality of life in patients with GBM [14], while at same time miss unrecognized high-risk recurrence voxels that are outside of 2cm boundary. Taking these reasons into consideration, it is necessary to more precisely deliver RT to voxels that are most at risk for recurrence.

Although there are some improvements in modern imaging, and our group has shown that incorporating metabolic and diffusion MRI techniques at the time of radiation therapy can be used to predict regions of subsequent recurrence, the accuracy of the likelihood of recurrence maps can still be improved and the process needs to be fully integrated with clinical RT planning work station. The automatic calculation of appropriate thresholds for automated contouring that has been demonstrated in this study can enable future for integration of metabolic and physiology imaging into the clinical workflow for radiation treatment planning potentially decreasing normal tissue toxicity and prolonging survival in patients with GBM.

While traditional standard RT treatment planning has an isotropic 2cm expansion of the

T2 hyperintensity lesion on the surgical resection cavity and residual tumor base on CEL and T2L

maps, we find regions that were likely to progress as far as 5cm way from the anatomical lesion

boundary. Although some voxels beyond this distance were also implicated, 5 cm is the maximum

distance from which our clinicians felt comfortable with treating with high dose. We successfully

incorporated this maximum distance (5cm) from the original lesion into our automated threshold

routine, which allowed for the automatic selection of a threshold from a consistent position on the

histogram of the probability maps from each patient that optimized the overlap probability maps

with the progressed lesion.

Because this patient cohort experienced a unique therapeutic strategy with concomitant

anti-angiogenic therapy at the time of RT, [15] [16] our thresholding procedure will need to be re-

optimized for GBM patients who received standard of care treatment [17] using the same

optimization approach. We expect that patients who did not receive anti-angiogenic therapy

would recur much closer to the original lesion and therefore not require such a large distance

threshold. The optimal histogram position is also likely to be shifted further to the right in patients

receiving standard of care therapy. New prediction models will also need to be generated for

different therapeutic regimes to determine whether the same imaging parameters are still relevant.

Although the preliminary results and framework demonstrate that the integration of

metabolic and physiology imaging into clinical workflow for radiation treatment planning is

encouraging, there are several potential limitations to this study. First, the sensitivity and

specificity of the optimal threshold for each patient varies among patients, with some patients

having relatively low sensitivity in part due to the accuracy of the original model and not precise

our automatic contouring method which works on the resulting probability maps. Automatic thresholding worked best when a good background to foreground contrast ratio existed, however, the often-gradual gradation in voxel intensity of the probability maps made it difficult to determine an obvious cutoff based on the probability map on its own. As a result, we used ROC curve analysis to help find optimal threshold by calculating the point on ROC curve that minimizes the Euclidean distance between the top left point (0,1) in ROC space [18] and the ROC curve [19]. This method is gives equal weight to sensitivity and specificity. Although we attempted to develop a strategy that worked best for the majority of the patients, an individual's contour may still need to be tweaked by the physicist or treating physician at the time of treatment planning.

CHAPTER 5

CONCLUSION

The preliminary results and images show that our pipeline for integration of metabolic and physiology imaging into clinical workflow for radiation treatment planning is encouraging. We were able to successfully develop an automated contouring routine that allowed the automatic selection of a threshold from a consistent position on the histogram of the probability maps that optimized the overlap with the progressed lesion and included a maximum distance from the original lesion. Although this patient cohort experienced a unique therapeutic strategy with anti-angiogenic therapy at the time of RT, the framework can be easily extended for RT planning of any patients with glioma treated with different therapeutic regimens. Future work will incorporate our results into the clinical RT treatment software and comparing with originally planned contours as shown in Figure 20. The original model used to generate a voxel-by-voxel risk of recurrence will also be improved by using deep learning to generate spatial maps that can more accurately predict the probability of recurrence in GBMs.
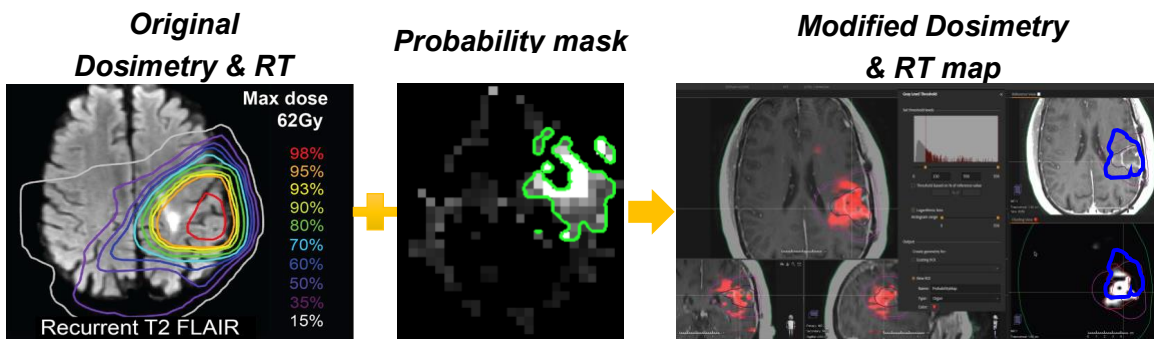

Figure 20. Incorporating a thresholded probability map into RT planning software

REFERENCES

[1] Bleeker, F. E., Molenaar, R. J., & Leenstra, S. (2012). Recent advances in the molecular understanding of glioblastoma. Journal of neuro-oncology, 108(1), 11-27.

[2] Fisher, J. L., Schwartzbaum, J. A., Wrensch, M., & Wiemels, J. L. (2007). Epidemiology of brain tumors. Neurologic clinics, 25(4), 867-890.

[3] Gallego, O. (2015). Nonsurgical treatment of recurrent glioblastoma. Current oncology, 22(4), e273.

[4] Anwar, M., Molinaro, A. M., Morin, O., Chang, S. M., Haas-Kogan, D. A., Nelson, S. J., & Lupo, J. M. (2017). Identifying Voxels at Risk for Progression in Glioblastoma Based on Dosimetry, Physiologic and Metabolic MRI. Radiation research, 188(3), 303-313.

[5] Nelson, S. J. (2011). Assessment of therapeutic response and treatment planning for brain tumors using metabolic and physiological MRI. NMR in biomedicine, 24(6), 734-749.

[6] Nelson, S. J., & Cha, S. (2003). Imaging glioblastoma multiforme. The Cancer Journal, 9(2), 134-145.

[7] Pirzkall, A., McKnight, T. R., Graves, E. E., Carol, M. P., Sneed, P. K., Wara, W. W., ... & Larson, D. A. (2001). MR-spectroscopy guided target delineation for high-grade gliomas. International Journal of Radiation Oncology* Biology* Physics, 50(4), 915-928.

[8] Park, I., Tamai, G., Lee, M. C., Chuang, C. F., Chang, S. M., Berger, M. S., ... & Pirzkall, A. (2007). Patterns of recurrence analysis in newly diagnosed glioblastoma multiforme after three-dimensional conformal radiation therapy with respect to pre–radiation therapy magnetic resonance spectroscopic findings. International Journal of Radiation Oncology* Biology* Physics, 69(2), 381-389.

[9] Chuang, C. F., Chan, A. A., Larson, D., Verhey, L. J., McDermott, M., Nelson, S. J., & Pirzkall, A. (2007). Potential value of MR spectroscopic imaging for the radiosurgical management of patients with recurrent high-grade gliomas. Technology in cancer research & treatment, 6(5), 375-382.

[10] "Detector Performance Analysis Using ROC Curves - MATLAB & Simulink Example". www.mathworks.com. Retrieved 11 August 2016.

[11] Gaspar, L. E., Fisher, B. J., Macdonald, D. R., Leber, D. V., Halperin, E. C., Schold, S. C., &

Cairncross, J. G. (1992). Supratentorial malignant glioma: patterns of recurrence and implications for external beam local treatment. International Journal of Radiation Oncology• Biology• Physics, 24(1), 55-57.

[12] Saraswathy, S., Crawford, F., & Nelson, S. J. (2006). Semi-automated segmentation of brain tumor lesions in MR images. In 14th Annual Meeting of ISMRM.

[13] Otsu, N. (1979). A threshold selection method from gray-level histograms. IEEE transactions on systems, man, and cybernetics, 9(1), 62-66.

[14] Cheng, J. X., Zhang, X., & Liu, B. L. (2009). Health-related quality of life in patients with high-grade glioma. Neuro-oncology, 11(1), 41-50.

[15] Chinot, O. L., Wick, W., Mason, W., Henriksson, R., Saran, F., Nishikawa, R., ... & Brandes, A. A. (2014). Bevacizumab plus radiotherapy–temozolomide for newly diagnosed glioblastoma. New England Journal of Medicine, 370(8), 709-722.

[16] Chinot, O., Wick, W., Mason, W., Henriksson, R., Sarn, F., & Nishikawa, R. (2012). Phase III Trial of Bevacizumab added to standard radiotherapy and temozolomide for newly-diagnosed glioblastoma: Final progression-free survival and interim overall survival results in Avaglio. Neuro-oncology, 14(suppl 6), vi101-vi105.

[17] Stupp, R., Mason, W. P., Van Den Bent, M. J., Weller, M., Fisher, B., Taphoorn, M. J., ... & Curschmann, J. (2005). Radiotherapy plus concomitant and adjuvant temozolomide for glioblastoma. New England Journal of Medicine, 352(10), 987-996.

[18] Unal, I. (2017). Defining an optimal cut-point value in roc analysis: an alternative approach. Computational and mathematical methods in medicine, 2017.

[19] Perkins Neil, J., & Schisterman Enrique, F. (2006). The Inconsistency of "Optimal" Cut-points Using Two ROC Based Criteria. Am J Epidemiol, 163, 670-675.

[20] Gogtay, N. J., & Thatte, U. M. (2017). Statistical Evaluation of Diagnostic Tests–Part 2 [Pre-test and post-test probability and odds, Likelihood ratios, Receiver Operating Characteristic Curve, Youden's Index and Diagnostic test biases]. Journal of The Association of Physicians of India, 65, 86.

Publishing Agreement

It is the policy of the University to encourage the distribution of all theses, dissertations, and manuscripts. Copies of all UCSF theses, dissertations, and manuscripts will be routed to the library via the Graduate Division. The library will make all theses, dissertations, and manuscripts accessible to the public and will preserve these to the best of their abilities, in perpetuity.

Please sign the following statement:

I hereby grant permission to the Graduate Division of the University of California, San Francisco to release copies of my thesis, dissertation, or manuscript to the Campus Library to provide access and preservation, in whole or in part, in perpetuity.

_____   2018. 09. 10
Author Signature   Date

32